

Domain Generalization through Attenuation of Domain-Specific Information

Reiji Saito Kazuhiro Hotta

Meijo University

200442065@ccalumni.meijo-u.ac.jp, kazuhotta@meijo-u.ac.jp

Abstract

In this paper, we propose a new evaluation metric called Domain Independence (DI) and Attenuation of Domain-Specific Information (ADSI) which is specifically designed for domain-generalized semantic segmentation in automotive images. DI measures the presence of domain-specific information: a lower DI value indicates strong domain dependence, while a higher DI value suggests greater domain independence. This makes it roughly where domain-specific information exists and up to which frequency range it is present. As a result, it becomes possible to effectively suppress only the regions in the image that contain domain-specific information, enabling feature extraction independent of the domain. ADSI uses a Butterworth filter to remove the low-frequency components of images that contain inherent domain-specific information such as sensor characteristics and lighting conditions. However, since low-frequency components also contain important information such as color, we should not remove them completely. Thus, a scalar value (ranging from 0 to 1) is multiplied by the low-frequency components to retain essential information. This helps the model learn more domain-independent features. In experiments, GTA5 (synthetic dataset) was used as training images, and a real-world dataset was used for evaluation, and the proposed method outperformed conventional approaches. Similarly, in experiments that the Cityscapes (real-world dataset) was used for training and various environment datasets such as rain and nighttime were used for evaluation, the proposed method demonstrated its robustness under nighttime conditions.

1. Introduction

Domain generalization aims to create models that are robust to unseen images that are not present in the training data, and recent research has achieved impressive results. SIMPLE [14] achieved the state-of-the-art performance by leveraging multiple pretrained models without fine-tuning

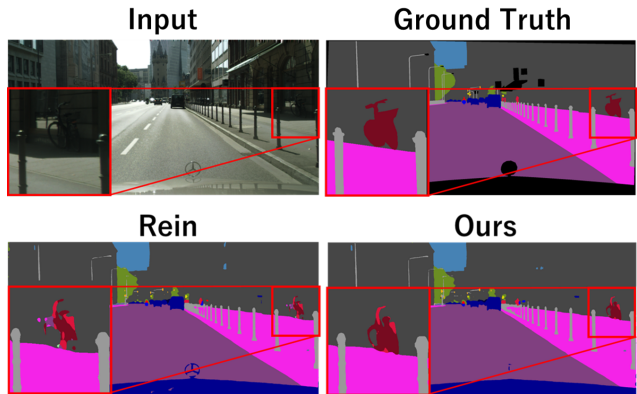


Figure 1. The areas improved by the proposed method are highlighted. The red box indicates a bicycle hidden in the shadow, making it quite difficult to see. As a result, the conventional method, Rein, fails to recognize the bicycle. However, by applying the proposed method (Ours), the bicycle hidden in the shadow becomes recognizable.

and selecting the most suitable pretrained model for each test sample. Similarly, domain generalization for semantic segmentation (DGSS) of automotive images, which we address in this paper, has improved in performance with the emergence of foundational models. Specifically, Rein [23] and VLTSeg [10] achieved high-performance results by fine-tuning foundation models such as DINOv2 [17] and vision-language models (VLMs) [19]. There are two types of domain generalization: one uses images from multiple domains (e.g. Photo and Sketch), and the other uses images from a single domain. For semantic segmentation, the high cost for obtaining ground-truth annotations often leads to use single-domain images or synthetic data. However, developing highly generalized models using only single-domain images remains challenging and is an active area of research.

The approach for using frequency domain has proven to be both simple and highly effective for domain adapta-

tion and domain generalization. In particular, methods such as FDA [26] and amplitude mix [25] improved the accuracy by swapping or mixing the low-frequency components of images from multiple domains. Low-frequency components contain domain-specific information, such as sensor characteristics and lighting differences, so replacing them helps mitigate distribution mismatches. Additionally, the RaffeSDG [13] method demonstrated generalization performance by attenuating low-frequency components separately for each color channel.

However, there are three issues with these methods. First, hyperparameters used in the experiment are determined through visualization or set implicitly, making it unclear where domain-specific information exists and to what extent it is considered. As a result, there is a possibility that the settings are overly optimized for the test data. Second, methods like FDA and amplitude mix assume the use of images from multiple domains. However, in domain generalization for in-vehicle images, training is conducted using only single-domain images, meaning that simply swapping or mixing low-frequency components does not necessarily improve generalization. This is because the sensor characteristics and lighting conditions remain consistent. Third, in the RaffeSDG method, low-frequency components are attenuated differently for each color channel when fundus images are used. However, for the in-vehicle image tasks addressed in this paper, we consider color information to be essential. This is because objects such as grass and sidewalks have similar shapes but are distinguishable by color, and losing this distinction could negatively impact predictions.

To address the first issue, this paper proposes a novel evaluation metric called “Domain Independence (DI)”, which measures the degree of domain dependency. If an image contains domain-specific information, the DI value is low, whereas if it consists only of domain-independent information, the DI value is high. By using DI, we can roughly determine where domain-specific information is present in the frequency space of an image (e.g. it exists in low or high frequencies, in amplitude or phase components). Furthermore, once the location of domain-specific information is identified by the proposed DI, it becomes possible to realize domain generalization from single domain.

To address the second and third issues, we propose “Attenuation of Domain-Specific Information (ADSI)”. ADSI is designed for realizing domain generalization from single domain by using DI metric to guide the hyperparameters. DI evaluation revealed that domain-specific information is primarily present in the low-frequency components of images. Thus, to mitigate domain-specific information, ADSI uses a Butterworth filter to remove the low-frequency components of images that contain domain-specific infor-

mation. Furthermore, to retain the color information in the low-frequency components that is important for the model’s predictions, we multiply the Butterworth filter by a randomly chosen scalar value between 0 and 1. Additionally, to maintain color consistency, ADSI applies the same scalar value to all color channels rather than using different values for each channel. This approach enables learning with domain-independent information, improving the robustness to unseen domains and enhancing generalization performance.

In experiments, we used GTA5 [20], which is a synthetic dataset, as training data and evaluated the generalization performance on real-world datasets such as Cityscapes [3], BDD [27], and Mapillary [16]. Additionally, we conducted experiments using Cityscapes as the training dataset and evaluated performance on ACDC [22], which includes challenging conditions such as rain and nighttime scenes. For comparison, we used Rein [23], a state-of-the-art domain generalization model known for its simplicity and high accuracy. As a result, in the experiments where GTA5 was used as training data, ADSI achieved an average mIoU improvement of 1.39% across all datasets compared to Rein. Furthermore, in the experiments where Cityscapes was used as training data, ADSI outperformed Rein by 3.26% mIoU on nighttime data, demonstrating its effectiveness in challenging conditions.

The main contributions of this paper are as follows.

- We propose “Domain Independence (DI)”. DI clarifies the regions containing domain-specific information and enables the quantitative setting of experimental parameters.
- We propose “Attenuation of Domain-Specific Information (ADSI)”, which can realize domain generalization from single domain.
- We conducted experiments across various DGSS tasks and demonstrated that the proposed ADSI achieved superior generalization performance compared to the state-of-the-art methods. Additionally, it was shown to outperform conventional methods, such as amplitude mix and RaffeSDG.

The structure of this paper is as follows. In Sec. 2, we discuss related works. Sec. 3 explains the details of the proposed method. In Sec. 4, we present experimental results and discussion. Finally, Sec. 5 concludes our paper and describes future challenges.

2. Related Works

Domain Generalization for Semantic Segmentation (DGSS) aims to build a robust model that can handle unknown domains not included in the training images. Unlike domain adaptation (DA), which focuses on a single target domain, DGSS requires the ability to generalize to any datasets. Previous methods have included normalization

techniques, whitening approaches, domain randomization, and strategies utilizing foundation models. For example, in the normalization-based approach IBN [18], instance normalization is used to learn domain-invariant features, while batch normalization is used to learn content-specific information. By carefully integrating these two types of normalization, IBN improved generalization capability. In RobustNet [2] which is the whitening-based approach, features that have changed due to optical transformations are selectively removed, thereby erasing domain-specific style information. With domain randomization, WildNet [12] diversifies style by making the source domain more similar to the style in the ImageNet [4] dataset. Finally, in methods based on foundation models, Rein examines the generalization performance of models such as CLIP [19] and DINOv2 [17], and it improved their generalization ability through fine-tuning.

However, these methods do not clarify where domain-specific information resides in the image or how it leads to performance degradation. Therefore, in this paper, we use the GTA5 and ImageNet datasets to identify which parts of an image contain domain-specific information. Moreover, inspired by RobustNet which selectively removes changes caused by optical properties, we use a Butterworth filter to remove low-frequency components that contain domain-specific information. However, since low-frequency components also include critical information for predictions, such as color information, we multiply them by a scalar value between 0 and 1, ensuring they are not entirely removed but effectively utilized.

3. Methodology

In this paper, we aim to improve the accuracy of DGSS. First, in Sec. 3.1, we propose an evaluation metric called “Domain Independence (DI)”. Next, in Sec. 3.2, we roughly determine which parts of an image contain domain-specific information. Finally, in Sec. 3.3, we propose an image transformation method for in-vehicle image DGSS, called “Attenuation of Domain-Specific Information (ADSI)”.

3.1. Domain Independence (DI)

In this paper, we roughly determine which parts of an image contain domain-specific information. First, Fig. 2 explains what domain-specific information is. In Fig. 2, two datasets (indicated in red and blue) are fed into the model, and the output features are visualized using t-SNE. Domain-specific information refers to the case where the two datasets are clustered separately, as shown on the left side of the figure. On the other hand, domain-independent information refers to the case where the two datasets are mixed. In other words, when the feature distances between different datasets are close, it indicates domain-independent information.

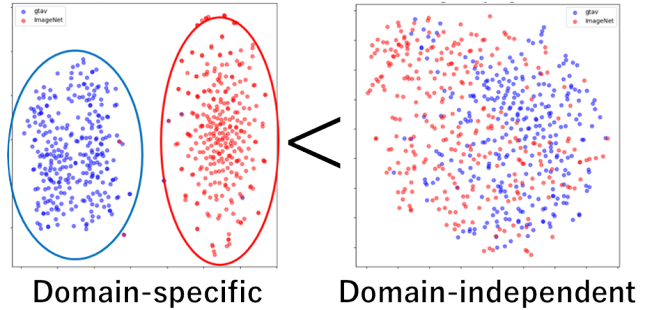


Figure 2. Definition of Domain-Specific and Domain-Independent. If the data has specific features to a particular domain, Domain-Independent metric will be low. On the other hand, if it does not contain domain-specific information, Domain-Independent metric will be high.

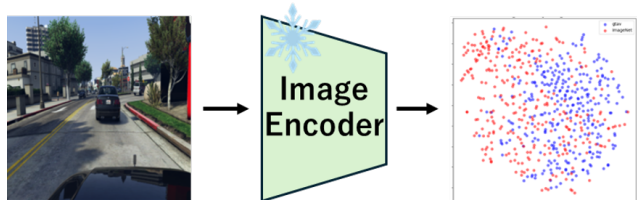


Figure 3. Overview of Domain Independence metric. The image is passed through a frozen Image Encoder to extract its features. The reason the image encoder is frozen is that it ensures consistent feature extraction, allowing roughly evaluation of differences between image domains. After that, by comparing the distances between features, the degree to which the image depends on a specific domain can be quantified.

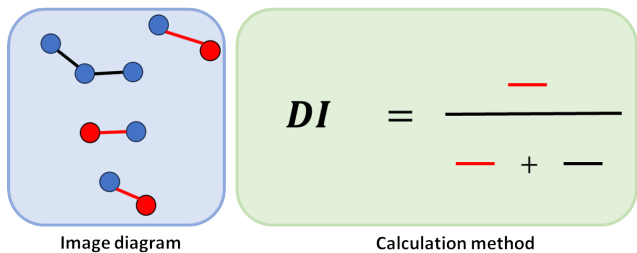


Figure 4. DI image diagram and calculation method. For a certain feature, if the closest feature values are in the same dataset, we count the black lines. On the other hand, if they are in different datasets, count the red lines.

Following this definition, we roughly determine where domain-specific information is present in the frequency space of images using the GTA5 dataset as the training data and the ImageNet dataset. We use ImageNet because it is a dataset of natural images with diverse styles, making it suitable for covering a wide range of image variations. Fig. 3

provides an overview of ‘‘Domain Independence (DI)’’.

First, we define the input image $x \in \mathbb{R}^{3 \times H \times W}$, where H and W represent the height and width, respectively. This image is fed into a pre-trained Vision Transformer (ViT) [5], and we obtain the output feature map $f \in \mathbb{R}^{N \times D}$ where N and D denote the number of patches and the embedding dimension, respectively. We extract B feature maps from the GTA5 and ImageNet datasets, resulting in a total of $2B$ feature maps. In this study, we set $B = 300$.

Next, we compute the pairwise distance matrix $P \in \mathbb{R}^{2B \times 2B}$. Excluding the diagonal elements of P , we determine the closest distance for each feature map. We assess the degree of domain independence based on whether the nearest feature map belongs to the same dataset or a different one. Specifically, for each feature map, if the nearest feature map is from the same dataset, we increment the denominator by 1. If it is from a different dataset, we increment both the numerator and the denominator by 1.

$$DI = \frac{M}{M + N} \quad (1)$$

where N and M are the counts of these occurrences, respectively.

The overview of Sec. 3.1 is illustrated in Fig. 4. A higher DI value indicates that the feature does not contain domain-specific information, while a lower DI value suggests the presence of domain-specific information.

3.2. Quantitative Evaluation of Domain-Specific Information

In this paper, we use DI to determine roughly which regions in the frequency space contain domain-specific information. The reason for analyzing the frequency space is that low-frequency amplitude components are believed to contain domain-specific information [26]. Therefore, we progressively remove low-frequency components to determine up to which frequency domain-specific information is retained. Additionally, we clarify whether the amplitude component, the phase component, or both in the frequency space contain domain-specific information.

3.2.1 Experiment on Removing Low-Frequency Components

We remove the low-frequency components of an image using a box and quantitatively evaluate the size of the box that contains domain-specific information using a domain information index (DI). First, we prepare an input image $x \in \mathbb{R}^{3 \times H \times W}$ and apply the Fast Fourier Transform (FFT) to obtain the frequency representation $F(x)$, which consists of amplitude and phase components.

$$\mathcal{F}(x)(m, n) = \sum_{h, w} x(h, w) e^{-j2\pi(\frac{h}{H}m + \frac{w}{W}n)}, \quad j^2 = -1 \quad (2)$$

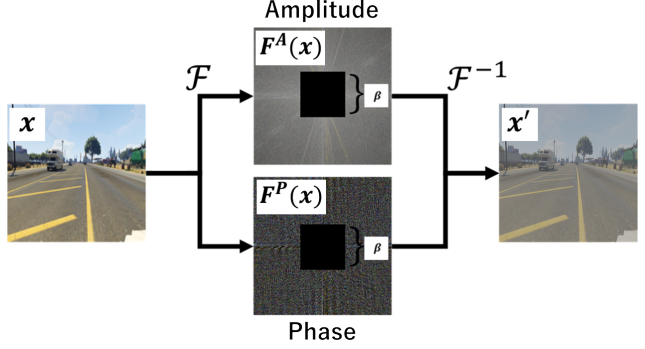


Figure 5. Overview of low-frequency component removal. By removing the frequency components inside the box, sensor characteristics and lighting conditions present in the low-frequency components can be eliminated. Since filters like the Butterworth filter gradually reduce the frequency components, it is not clear where the domain-specific information is contained. Therefore, here we use a box filter to clearly eliminate the frequency components in specific areas. Additionally, by adjusting β , the size of the box can be modified.

where (h, w) represents the spatial coordinates of the image, while (m, n) represents the coordinates in the frequency domain.

Next, we apply a Box filter and create a mask where the inside of the Box is set to 0 and the outside is set to 1.

$$M_\beta(h, w) = 1 - 1_{(h, w) \in [-\beta H: \beta H, -\beta W: \beta W]} \quad (3)$$

where $\beta \in (0, 1)$, and the center of the image is assumed to be $(0, 0)$. The specified low-frequency components are removed by multiplying the mask with the amplitude and phase components of $F(x)$. Then, an inverse Fourier transform (IFFT) is applied to reconstruct the image with the low-frequency components removed. These processes are illustrated in Fig. 5.

$$x' = \mathcal{F}^{-1} [M_\beta \circ \mathcal{F}^A(x), M_\beta \circ \mathcal{F}^P(x)] \quad (4)$$

where \mathcal{F}^A and \mathcal{F}^P represent the amplitude and phase components of the Fourier transform, respectively, while \mathcal{F}^{-1} denotes the inverse Fourier transform. The reconstructed image after the inverse Fourier transform is denoted as x' .

We analyze the influence of low-frequency components by performing a quantitative evaluation using DI on the reconstructed images. Furthermore, by gradually increasing the Box size (β), we can determine up to which frequency components retain domain-specific information. Fig. 6 illustrates an experiment in which DI is used to quantitatively evaluate up to which frequency band an image retains its domain-specific characteristics. The horizontal axis represents the ratio (β) of the box size to the image size, while the vertical axis indicates the proposed DI value. Observing Fig. 6, we can see that the DI value increases from 0 to

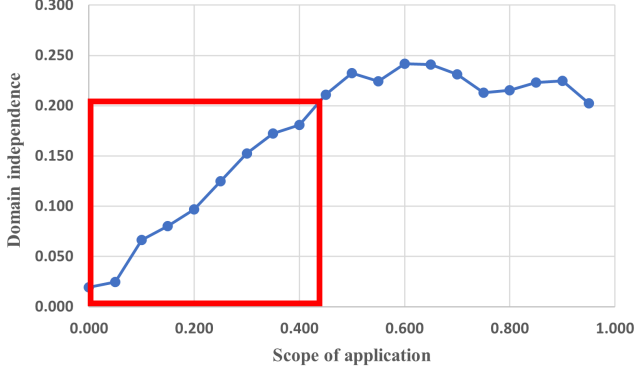


Figure 6. An experiment was conducted to quantitatively evaluate domain independence using the proposed DI, up to which frequency band an image retains its domain-specific characteristics. The areas enclosed by the red box indicate the regions that exhibit domain-specific characteristics.

0.4 on the horizontal axis. However, when the horizontal axis value exceeds 0.4, the DI value becomes nearly constant. These results suggest that the frequency band up to 0.4 times the image size retains domain-specific characteristics, and applying processing to this region can effectively mitigate domain-specific information. Therefore, in this experiment, the value of β is set between 0 and 0.4.

3.2.2 Comparison of Domain Independence Between Amplitude and Phase Components

Conventional methods such as FDA and amplitude mix apply Fourier transform to images, process only the amplitude components, and then reconstruct the images for training. The phase components were not processed because they were considered to contain high-level semantics and were believed to be unaffected by domain shifts. However, does domain shift truly not occur? To investigate this, we conduct a quantitative evaluation using Domain Invariance (DI) with images reconstructed from only the amplitude components and only the phase components.

We conducted an evaluation using Domain Invariance (DI) with images reconstructed from only the amplitude components and only the phase components. DI values were 0.19 for the amplitude-only reconstruction and 0.10 for the phase-only reconstruction. From these results, it is confirmed that the phase components contain intrinsic domain-specific information. Therefore, by applying a filter to both the amplitude and phase components, we can mitigate domain-specific information.

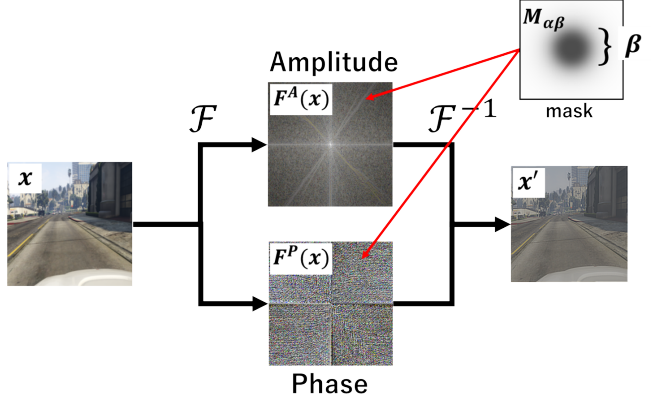


Figure 7. Overview of the Proposed Method. The proposed method applies a Fourier transform to the input image and multiplies both the amplitude and phase components by M_b . This process removes low-frequency components that contain domain-specific information, such as sensor characteristics. Then, the image is reconstructed using the inverse Fourier transform. By training with these reconstructed images, the model can make predictions that are independent of domain-specific information.

3.3. Attenuation of Domain-Specific Information (ADSI)

We propose “Attenuation of Domain-Specific Information (ADSI)”, in which domain generalization is obtained from a single domain. Fig. 7 illustrates the overview of ADSI. First, we define the input image x and perform a fast Fourier transform using Eq. 2. Next, as shown in Secs. 3.2.1 and 3.2.2, domain-specific information exists in both the amplitude and phase components within the frequency band where β is up to 0.4. Therefore, to suppress the influence of low-frequency components in both the amplitude and phase components, we create a mask. However, unlike M_β , we use a Butterworth filter. This is because ringing artifacts appear in the output image x' in Fig. 5. Regarding the consistency with the experiment in Fig. 6, it differs slightly when a Box is used, but the overall aspects remain unchanged. The cause of the ringing artifacts is the gap that occurs when the low-frequency components are removed by the Box filter. The mask using a Butterworth filter can be expressed by the following equation.

$$M'_\beta = \frac{1}{1 + \left(\frac{\sqrt{h^2 + w^2}}{\beta + \epsilon}\right)^{2N}} \quad (5)$$

where the center coordinate refers to $(0, 0)$, $\beta \in (0, 0.4)$, $N \in (1, 3)$ same as RaffeSDG [13] and ϵ represents a small value. M'_β is close to 1 for low-frequency components and close to 0 for high-frequency components. In segmentation using in-vehicle images, color information is also necessary. Therefore, to avoid removing low-frequency com-

ponents completely that contain color information, a random scalar value between 0 and 1 is multiplied by the mask. Then, this mask retains the low-frequency components and removes the high-frequency components. By subtracting 1, the high-frequency components are preserved, and the influence of the low-frequency components is reduced. The mask can be expressed by the following equation.

$$M_{\alpha\beta} = 1 - \alpha \circ M'_{\beta} \quad (6)$$

where $\alpha \in (0, 1)$. By using Eq. 4, $M_{\alpha\beta}$ is applied to the amplitude and phase components, and finally an inverse Fourier transform is performed to obtain the output image x' . By using the output image, learning can be conducted with domain-independent information, enabling robust predictions even for unseen data.

4. Experiments

4.1. Settings

Datasets. We evaluate the proposed method and existing methods using synthetic datasets (GTA5 [20], Synthia [21]) and real-world datasets (Cityscapes [3] (Citys), BDD100K [27] (BDD), Mapillary [16] (Map), ACDC [22]). The GTA5 dataset consists of 24,966 synthetic images obtained from a game with pixel-level annotations. The Synthia dataset contains 9,400 annotated images rendered from a virtual city. The Cityscapes dataset is an autonomous driving dataset that includes 2,975 training images and 500 validation images. Similarly, the BDD100K and Mapillary datasets provide 1,000 and 2,000 validation image for perception algorithms in autonomous driving. The ACDC dataset includes challenging conditions such as fog, nighttime, rain, and snow, with validation data consisting of 106 images for nighttime and 100 images for each of the other conditions. In addition, to ensure consistency in training data, all datasets are aligned to match the Cityscapes 19 class format.

Implementation details. We conduct experiments using Rein [23] as the baseline. Rein is a state-of-the-art method that utilizes various image foundation models, such as CLIP [19] and SAM [11], as the backbone and employs Mask2Former [1] for the segmentation head. Therefore, we will use Rein (with DINOv2 [17] as the backbone) as the baseline and evaluate the performance when we incorporate the proposed method into the baseline. The experimental setup follows that of Rein, using AdamW [15] as the optimization method. The learning rate is set to $1 \times e^{-5}$ for the backbone and $1 \times e^{-4}$ for Rein and the segmentation head. Training is conducted for 40,000 iterations with a batch size of 4, and images are cropped to 512×512 . Data augmentation follows the same approach as Rein with ADSI when the proposed method is used. The evaluation metric is Intersection over Union (IoU). The values presented in Tables represent the mean IoU. The experiments were conducted

Table 1. Comparison with state-of-the-art methods. The model was trained on the GTA5 dataset and evaluated on real-world dataset. Additionally, Avg. represents the average value across Cityscapes (Citys), BDD100K (BDD), and Mapillary (Map).

Method	Backbone	GTA5-to-Real			
		Citys	BDD	Map	Avg.
IBN [18]	RN50 [7]	33.61	32.67	37.43	34.57
ISW [2]	RN50	36.40	35.79	40.30	37.50
WildNet [12]	RN101	44.62	38.35	46.09	43.02
DAFormer [8]	MiT-B5 [24]	52.88	47.37	54.34	51.53
HRDA [9]	MiT-B5	57.45	49.10	59.92	55.49
VLTSeg [10]	EVA02-CLIP-L [6]	65.30	58.30	66.0	63.20
Rein [23]	CLIP-L [19]	58.35	54.75	59.91	57.67
Rein	SAM-H [11]	59.66	50.03	61.14	54.94
Rein	EVA02-CLIP-L	63.23	59.63	63.81	62.22
Rein	DINOv2-L [17]	66.12	60.51	65.90	64.18
RaffeSDG [13]	DINOv2-L	61.78	58.98	62.72	61.16
FACT [25]	DINOv2-L	64.75	60.27	64.66	63.23
Ours	DINOv2-L	67.75	61.38	67.59	65.57

Table 2. Comparison with the baseline (Rein) when we trained on Cityscapes (Citys) and evaluated on the ACDC dataset which contains data from various environmental conditions.

Method	Backbone	Citys-to-ACDC				
		Night	Snow	Fog	Rain	Avg.
Rein	DINOv2-L	55.56	72.13	81.09	75.19	70.99
Ours	DINOv2-L	58.82	71.07	81.17	69.19	70.21

using a single RTX A6000 GPU for training. For comparison with the baseline, we used DINOv2-Large.

4.2. Quantitative Evaluation

Tab. 1 presents the results of training on the synthetic dataset GTA5 and evaluating on the real-world datasets Citys, BDD, and Map. The baseline method, Rein-DINOv2-L, achieves better accuracy compared to other conventional approaches. Additionally, the conventional methods such as RaffeSDG and FACT were trained using Rein-DINOv2-L but resulted in lower accuracy. This decline in performance may be attributed to the removal or alteration of color information, which negatively impacted predictions. On the other hand, the proposed method (Ours) achieved accuracy improvements of 2.63% on Citys, 0.87% on BDD, and 1.69% on Map compared to the baseline Rein-DINOv2-L. This demonstrated that our method successfully learned domain-independent features while preserving color information, leading to better generalization performance on real-world data.

Tab. 2 evaluates whether the model trained on Citys generalizes well across various environmental conditions. Since Rein-DINOv2-L achieved the best accuracy among conventional domain generalization methods in Table 1, we compare only with Rein-DINOv2-L. The results show that Ours improved the accuracy by 3.26% in the Night scenario compared to Rein-DINOv2-L. This significant improve-

Table 3. Comparison with the baseline (Rein) when we trained on synthetic datasets: GTA5 and Synthia, and evaluated on Cityscapes (Citys), BDD100K (BDD), and Mapillary (Map) datasets. The accuracy improved when Synthia was included in comparison with only GTA5 for training. Furthermore, Ours outperformed Rein.

Method	Backbone	GTA5+Synthia-to-Real			
		Citys	BDD	Map	Avg.
Rein	DINOv2-L	66.91	60.87	67.94	65.24
Ours	DINOv2-L	69.03	61.76	68.26	66.35

Table 4. Comparison with the baseline (Rein) when trained on GTA5 and evaluated on the ACDC dataset, which contains data from various environmental conditions.

Method	Backbone	GTA5-to-ACDC				
		Night	Snow	Fog	Rain	Avg.
Rein	DINOv2-L	49.40	64.74	72.19	61.63	61.99
Ours	DINOv2-L	50.37	66.69	72.44	64.57	63.52

ment in Night conditions may be due to reducing the influence of low-frequency components, which helps the model better capture nighttime environments. However, in other conditions, the accuracy either remained nearly the same or worsened. This may be because reducing low-frequency components led to a prediction bias toward high-frequency features. Since high-frequency components contain the details such as fog or raindrops, and the model was not explicitly trained to handle such domain shifts, this likely resulted in the observed performance drop.

Tab. 3 presents the results when the Synthia dataset was additionally included in training, building upon the results in Tab. 1. We conducted this experiment to verify whether increasing synthetic data further enhances the effectiveness of our method. The Rein-DINOv2-L in Tab. 3 achieved better accuracy than the Rein-DINOv2-L in Tab. 1. Furthermore, Ours outperformed conventional methods, demonstrating its effectiveness. However, the improvement in accuracy was smaller than the case that only the GTA5 dataset was used for training. These results indicate that our method remains applicable even when additional synthetic data is introduced, reinforcing its robustness.

Tab. 4 evaluates whether the model trained on the GTA5 dataset can generalize over various environmental conditions. While Tab. 2 examined generalization when we trained on real-world data (Citys), our method is trained on synthetic data in this experiment. The results show that Ours outperforms conventional methods, demonstrating superior accuracy. These findings indicate that the usage of synthetic data leads to performance improvements in all environmental conditions. This improvement may be attributed to our method’s ability to remove the characteristic textures of synthetic data, making the model more robust to

Table 5. The baseline is Rein-DINOv2-L, and the comparison is made when various methods are used for removing low-frequency components. “Box (Amplitude)” refers to the method in Fig. 5, where only the amplitude of the low-frequency components is removed by adopting a factor α , effectively either removing or keeping the low-frequency components. “Box” follows the same approach as Fig. 5 but it multiplies $\alpha \in (0, 1)$ with M_b of Eq. 3 to randomly remove low-frequency components, “Circle” is a variation where “Box” is modified into a Circle. “Color” is created by generating a mask of Ours separately for each color channel and multiplying it with the frequency components. “Butter (Amplitude)” is our proposed method applied only to the amplitude components.

Method	Backbone	GTA5-to-Real			
		Citys	BDD	Map	Avg.
Rein	DINOv2-L	66.12	60.51	65.90	64.18
Box (Amplitude)	DINOv2-L	66.27	61.21	66.0	64.49
Box	DINOv2-L	67.19	61.14	66.22	64.85
Circle	DINOv2-L	67.04	60.34	66.68	64.69
Color	DINOv2-L	67.39	60.08	66.66	64.69
Butter (Amplitude)	DINOv2-L	66.84	61.56	66.50	64.97
Ours	DINOv2-L	67.75	61.38	67.59	65.57

domain shifts.

4.3. Qualitative Evaluation

Fig. 8 shows the visualization results by models trained on GTA5 and evaluated on Cityscapes, BDD, and Map (GTA5 \rightarrow Avg.), as well as models trained on Cityscapes and evaluated on Night and Rain (Cityscapes \rightarrow ACDC). From left to right, each column represents the input image, ground truth, the baseline model (Rein-DINOv2-L), and our proposed method (Ours). The orange boxes highlight the improved regions, while the blue boxes indicate degraded areas.

In Cityscapes, focusing on the orange boxes, we observe that Rein-DINOv2-L misclassifies the bicycle class as vegetation due to domain shift. In contrast, while it is not perfect, Ours can recognize the bicycle class to some extent. This suggests that our method enables prediction based on domain-independent information.

In Rain, when we focus on the blue boxes, we see that Ours misclassifies the bus as a truck while Rein-DINOv2-L correctly recognizes the bus class. This is likely because Ours focuses on high-frequency components for predictions. However, raindrops in the input image also contain high-frequency components, making it difficult for our model to adapt to the domain shift caused by the training data distribution.

4.4. Ablation Studies and Analysis

We evaluate our method by various ablation studies. The results are shown in Sec. 4.4. Note that the baseline is Rein, and “Box” follows the same approach as Fig. 5, where a

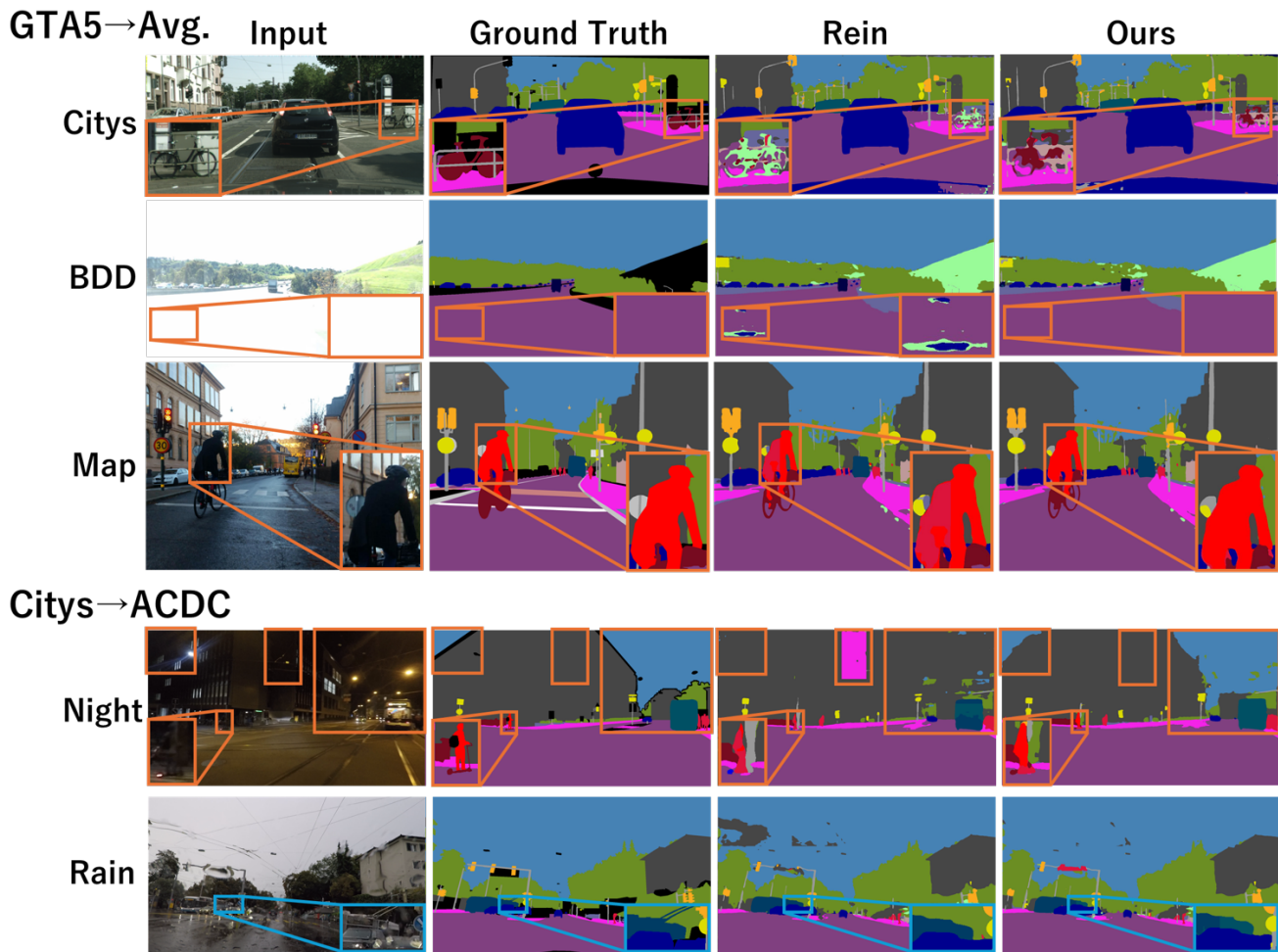


Figure 8. The visualization results by baseline model (Rein) and our method (Ours). The results show models trained on GTA5 and evaluated on Cityscapes, BDD, and Map (GTA5 → Avg.), as well as models trained on Cityscapes and evaluated on Night and Rain (Cityscapes → ACDC). From left to right, the columns represent Input, Ground Truth, Rein-DINOv2-L, and Ours. The orange boxes highlight improved regions, while the blue boxes indicate degraded areas.

factor α is multiplied by the low-frequency components to either remove or retain them. “Circle” is a circular version of Box. “Color” is created by generating a mask of Ours separately for each color channel and multiplying it with the frequency components. For methods labeled with “Amplitude”, the adjustment is applied only to the amplitude and not to the phase.

As a result, all methods outperformed the baseline. In addition, Ours achieved the best performance. “Box” and “Circle” did not significantly improve the accuracy due to the presence of ringing artifacts. Furthermore, by applying the augmentation to both amplitude and phase, Ours gave better results than applying it to amplitude alone. This suggests that the phase also has a unique domain, which is consistent with the experimental results in Sec. 3.2.2. More-

over, “Color” applied different masks to each color channel, causing color changes, which likely reduced its effectiveness.

5. Conclusion

In this paper, we propose DI and ADSI, demonstrating superior results compared to state-of-the-art methods and conventional augmentation techniques. However, our approach did not perform well in rainy and snowy environments during domain generalization, where the model was trained on Cityscapes and evaluated on ACDC. Since raindrops and snow are associated with high-frequency components that contain fine details, we plan to further investigate high-frequency components and will improve our method.

References

- [1] Bowen Cheng, Ishan Misra, Alexander G. Schwing, Alexander Kirillov, and Rohit Girdhar. Masked-attention transformer for universal image segmentation. In *Proceedings of the IEEE/CVF Conference on Computer Vision and Pattern Recognition (CVPR)*, pages 1290–1299, 2022. 6
- [2] Sungha Choi, Sanghun Jung, Huiwon Yun, Joanne T Kim, Seungryong Kim, and Jaegul Choo. Robustnet: Improving domain generalization in urban-scene segmentation via instance selective whitening. In *Proceedings of the IEEE/CVF conference on computer vision and pattern recognition*, pages 11580–11590, 2021. 3, 6
- [3] Marius Cordts, Mohamed Omran, Sebastian Ramos, Timo Rehfeld, Markus Enzweiler, Rodrigo Benenson, Uwe Franke, Stefan Roth, and Bernt Schiele. The cityscapes dataset for semantic urban scene understanding. In *Proc. of the IEEE Conference on Computer Vision and Pattern Recognition (CVPR)*, 2016. 2, 6
- [4] Jia Deng, Wei Dong, Richard Socher, Li-Jia Li, Kai Li, and Li Fei-Fei. Imagenet: A large-scale hierarchical image database. In *2009 IEEE Conference on Computer Vision and Pattern Recognition*, pages 248–255, 2009. 3
- [5] Alexey Dosovitskiy, Lucas Beyer, Alexander Kolesnikov, Dirk Weissenborn, Xiaohua Zhai, Thomas Unterthiner, Mostafa Dehghani, Matthias Minderer, Georg Heigold, Sylvain Gelly, Jakob Uszkoreit, and Neil Houlsby. An image is worth 16x16 words: Transformers for image recognition at scale. In *International Conference on Learning Representations*, 2021. 4
- [6] Yuxin Fang, Quan Sun, Xinggong Wang, Tiejun Huang, Xinlong Wang, and Yue Cao. Eva-02: A visual representation for neon genesis. *Image and Vision Computing*, page 105171, 2024. 6
- [7] Kaiming He, Xiangyu Zhang, Shaoqing Ren, and Jian Sun. Deep residual learning for image recognition. In *Proceedings of the IEEE Conference on Computer Vision and Pattern Recognition (CVPR)*, 2016. 6
- [8] Lukas Hoyer, Dengxin Dai, and Luc Van Gool. Daformer: Improving network architectures and training strategies for domain-adaptive semantic segmentation. In *Proceedings of the IEEE/CVF Conference on Computer Vision and Pattern Recognition (CVPR)*, pages 9924–9935, 2022. 6
- [9] Lukas Hoyer, Dengxin Dai, and Luc Van Gool. HRDA: Context-aware high-resolution domain-adaptive semantic segmentation. In *Proceedings of the European Conference on Computer Vision (ECCV)*, pages 372–391, 2022. 6
- [10] Christoph Hümmer, Manuel Schwonberg, Liangwei Zhou, Hu Cao, Alois Knoll, and Hanno Gottschalk. Strong but simple: A baseline for domain generalized dense perception by clip-based transfer learning. In *ACCV*, 2024. 1, 6
- [11] Alexander Kirillov, Eric Mintun, Nikhila Ravi, Hanzi Mao, Chloe Rolland, Laura Gustafson, Tete Xiao, Spencer Whitehead, Alexander C. Berg, Wan-Yen Lo, Piotr Dollar, and Ross Girshick. Segment anything. In *Proceedings of the IEEE/CVF International Conference on Computer Vision (ICCV)*, pages 4015–4026, 2023. 6
- [12] Suhyeon Lee, Hongje Seong, Seongwon Lee, and Euntai Kim. Wildnet: Learning domain generalized semantic segmentation from the wild. In *Proceedings of the IEEE/CVF conference on computer vision and pattern recognition*, pages 9936–9946, 2022. 3, 6
- [13] Heng Li, Haojin Li, Jianyu Chen, Zhongxi Qiu, Huazhu Fu, Lidai Wang, Yan Hu, and Jiang Liu. Rafflesdg: Random frequency filtering enabled single-source domain generalization for medical image segmentation. *arXiv preprint arXiv:2405.01228*, 2024. 2, 5, 6
- [14] Ziyue Li, Kan Ren, Xinyang Jiang, Yifei Shen, Haipeng Zhang, and Dongsheng Li. Simple: Specialized model-sample matching for domain generalization. In *The Eleventh International Conference on Learning Representations*. 1
- [15] Ilya Loshchilov and Frank Hutter. Decoupled weight decay regularization. In *International Conference on Learning Representations*, 2019. 6
- [16] Gerhard Neuhold, Tobias Ollmann, Samuel Rota Buló, and Peter Kotschieder. The mapillary vistas dataset for semantic understanding of street scenes. In *Proceedings of the IEEE international conference on computer vision*, pages 4990–4999, 2017. 2, 6
- [17] Maxime Oquab, Timothée Darcet, Théo Moutakanni, Huy V. Vo, Marc Szafraniec, Vasil Khalidov, Pierre Fernandez, Daniel HAZIZA, Francisco Massa, Alaaeldin El-Nouby, Mido Assran, Nicolas Ballas, Wojciech Galuba, Russell Howes, Po-Yao Huang, Shang-Wen Li, Ishan Misra, Michael Rabbat, Vasu Sharma, Gabriel Synnaeve, Hu Xu, Herve Jegou, Julien Mairal, Patrick Labatut, Armand Joulin, and Piotr Bojanowski. DINOv2: Learning robust visual features without supervision. *Transactions on Machine Learning Research*, 2024. Featured Certification. 1, 3, 6
- [18] Xingang Pan, Ping Luo, Jianping Shi, and Xiaoou Tang. Two at once: Enhancing learning and generalization capacities via ibn-net. In *Proceedings of the european conference on computer vision (ECCV)*, pages 464–479, 2018. 3, 6
- [19] Alec Radford, Jong Wook Kim, Chris Hallacy, Aditya Ramesh, Gabriel Goh, Sandhini Agarwal, Girish Sastry, Amanda Askell, Pamela Mishkin, Jack Clark, et al. Learning transferable visual models from natural language supervision. In *International conference on machine learning*, pages 8748–8763. PMLR, 2021. 1, 3, 6
- [20] Stephan R. Richter, Vibhav Vineet, Stefan Roth, and Vladlen Koltun. Playing for data: Ground truth from computer games. In *European Conference on Computer Vision (ECCV)*, pages 102–118. Springer International Publishing, 2016. 2, 6
- [21] German Ros, Laura Sellart, Joanna Materzynska, David Vazquez, and Antonio M. Lopez. The synthia dataset: A large collection of synthetic images for semantic segmentation of urban scenes. In *2016 IEEE Conference on Computer Vision and Pattern Recognition (CVPR)*, pages 3234–3243, 2016. 6
- [22] Christos Sakaridis, Dengxin Dai, and Luc Van Gool. Acdc: The adverse conditions dataset with correspondences for semantic driving scene understanding. In *Proceedings of the IEEE/CVF International Conference on Computer Vision*, pages 10765–10775, 2021. 2, 6

- [23] Zhixiang Wei, Lin Chen, Yi Jin, Xiaoxiao Ma, Tianle Liu, Pengyang Ling, Ben Wang, Huaian Chen, and Jinjin Zheng. Stronger fewer & superior: Harnessing vision foundation models for domain generalized semantic segmentation. In *Proceedings of the IEEE/CVF Conference on Computer Vision and Pattern Recognition (CVPR)*, pages 28619–28630, 2024. 1, 2, 6
- [24] Enze Xie, Wenhai Wang, Zhiding Yu, Anima Anandkumar, Jose M Alvarez, and Ping Luo. Segformer: Simple and efficient design for semantic segmentation with transformers. *Advances in neural information processing systems*, 34: 12077–12090, 2021. 6
- [25] Qinwei Xu, Ruipeng Zhang, Ya Zhang, Yanfeng Wang, and Qi Tian. A fourier-based framework for domain generalization. In *Proceedings of the IEEE/CVF conference on computer vision and pattern recognition*, pages 14383–14392, 2021. 2, 6
- [26] Yanchao Yang and Stefano Soatto. Fda: Fourier domain adaptation for semantic segmentation. In *Proceedings of the IEEE/CVF conference on computer vision and pattern recognition*, pages 4085–4095, 2020. 2, 4
- [27] Fisher Yu, Haofeng Chen, Xin Wang, Wenqi Xian, Yingying Chen, Fangchen Liu, Vashisht Madhavan, and Trevor Darrell. Bdd100k: A diverse driving dataset for heterogeneous multitask learning. In *Proceedings of the IEEE/CVF conference on computer vision and pattern recognition*, pages 2636–2645, 2020. 2, 6